Microbial Biotechnology

WILEY

MICROBIAL BIOTECHNOLOGY Open Access

RESEARCH ARTICLE OPEN ACCESS

A Single-Plasmid Inducible-Replication System for High-Yield Production of Short Ff (f1, M13 or fd)-Phage-Derived Nanorods

Rayén Ignacia León-Quezada[1,2] | Majela González Miró[1] | Sofia Khanum[1] | Andrew J. Sutherland-Smith[1] | Vicki A. M. Gold[3,4] | Jasna Rakonjac[1,2]

[1]School of Food Technology and Natural Sciences, Massey University, Manawatū Campus, Palmerston North, New Zealand | [2]Nanophage Technologies Ltd., Palmerston North, New Zealand | [3]Living Systems Institute, University of Exeter, Exeter, UK | [4]Faculty of Health and Life Sciences, University of Exeter, Exeter, UK

Correspondence: Jasna Rakonjac (j.rakonjac@massey.ac.nz)

Received: 1 November 2024 | **Revised:** 31 January 2025 | **Accepted:** 7 February 2025

Funding: This work was supported by V.A.M.G. from a Wellcome (Seed Award in Science; 210363/Z/18/Z) and to J.R. from Anonymous Donor, Palmerston North Medical Research Foundation, Massey University Research Fund and School of Natural Sciences; Royal Society Te Apārangi; Marsden Fund (03-MAU-210).

Keywords: DNA origami | f1 phage | fd phage | filamentous bacteriophages | M13 phage | nanoparticles | nanorods

ABSTRACT

Ff (f1, M13 or fd) filamentous phages have been used for myriad applications including phage display, assembly of nanostructures and as carriers of agents used for diagnostic and therapeutic purposes. Recently, short Ff phage-derived functionalised nanorods have emerged as a superior alternative to full-length filamentous phages for applications from lateral flow assays to cell- and tissue-targeting. Their advantages, such as shorter length and the lack of antibiotic resistance genes, make them particularly promising for expanding the current scope of Ff bionanotechnology and biomedical applications. Limitations to the widespread use of Ff-derived nanorods include a requirement for two plasmids and the relatively low production efficiency. This is due to the presence of only the positive Ff origin of replication, allowing replication of only the positive strand. Here we describe a single-plasmid negative origin-containing inducible-replication system for nanorod production. These improvements simplify and increase nanorod production by two orders of magnitude compared with the constitutive positive origin-only production system. The high concentration of nanorods allows formation of higher-order structures, such as stacks and rafts, as imaged by transmission electron microscopy. In summary, our system will facilitate production and expand the applications of Ff-derived biological nanorods.

1 | Introduction

Filamentous bacteriophages are a widespread group of long filament-like bacterial viruses (Mai-Prochnow et al. 2015; Rakonjac 2022; Roux et al. 2019). Three nearly identical filamentous phages, f1, M13 and fd, collectively known as Ff, infect *Escherichia coli* via the F pilus. Ff has been instrumental in the development of sophisticated vectors and functionalised viral particles, and as such is the workhorse of phage display technology, protein engineering and nanotechnology (Mao et al. 2004; McCafferty et al. 1990; Scott and Smith 1990; Smith 1985).

Filamentous phages replicate by a rolling circle mechanism, one strand at a time (Model and Russel 1988; Rakonjac et al. 2024). Circular (+) strand (single-stranded) DNA (cssDNA), synthesised with the help of the phage-encoded protein pII and (+) strand

origin of replication *(+) ori* (Horiuchi 1997), is packaged into phage and phage-derived particles via a secretion-like process across the host's envelope, allowing the host to survive (Conners et al. 2021; Haase et al. 2022; Rakonjac et al. 2024). The phage-encoded transenvelope assembly machinery is composed of a multimeric ATPase called pI/pXI in the cytoplasmic membrane, which interacts with an outer membrane multimeric channel of the secretin family called pIV (Figure 1). Assembly is initiated by the interaction of a hairpin loop in cssDNA, called the packaging signal (PS), with two minor virion proteins, pVII and pIX, at the cytoplasmic membrane. This is followed by an elongation step when the subunits of major coat protein pVIII associate along the quasi-Watson-Crick helix formed by the cssDNA (Russel and Model 1989). Once the end of the cssDNA reaches the assembly machinery, the virion is released from the cell by the addition of minor coat proteins pVI and pIII (Conners et al. 2023; Rakonjac et al. 1999). The length of filamentous phages and their derived particles thus depends on the length of the packaged cssDNA, which is in turn replicated from the *(+) ori* (Figure S1). Given that cssDNA ([+] strand) replication is initiated and terminated at a single pII cut site within the phage genome, cssDNA that is packaged into the virion corresponds to the complete genome (Horiuchi 1997). Similarly, Ff-like particles produced using vectors containing the complete Ff origin of replication and packaging signal as a backbone (also called phagemids) correspond to the size of the complete replicon (Vieira and Messing 1987).

Due to their spaghetti-like filamentous shape (6 nm × ~1 μm) and the presence of an antibiotic resistance gene within the genome of filamentous phage-derived vectors, they are not suitable for applications that depend on diffusion or involve release from laboratory confinement. This limitation affects their use in disposable sensors, rapid tests, medical therapeutics, prophylactics and diagnostics.

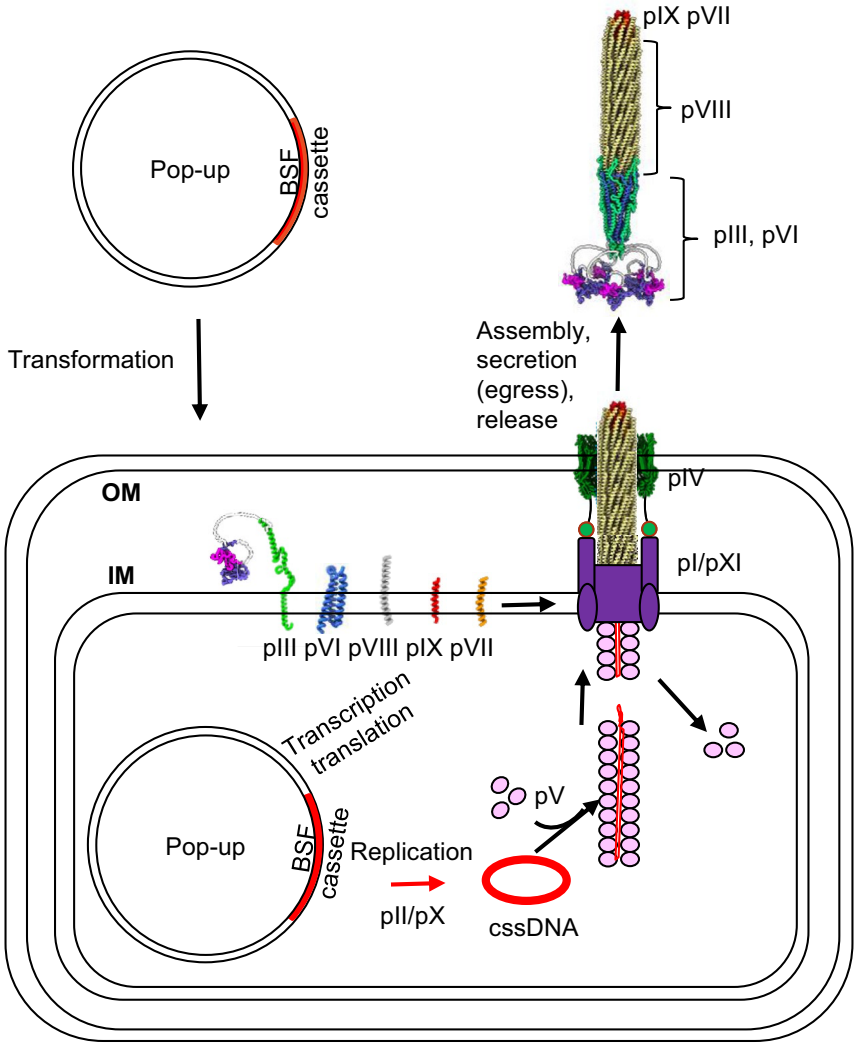

FIGURE 1 | Single-plasmid nanorod production system. Pop-up, single plasmid for nanorod production. BSF cassette (red), short for BSF replication-assembly cassette, a plasmid fragment that is replicated and converted to a short circular single-stranded DNA serving as a template for assembly of nanorods. BSF stands for Biological Scalable Ff-derived (nanorods). OM, outer membrane; IM, inner membrane, cssDNA, (+)-strand single-stranded circular DNA backbone of the nanorod. pIII, pVI, pVIII, pVII, pIX, Ff virion proteins encoded by the Pop-up plasmid. The nanorod image was derived from the cryoEM structures 8B3O, 8B3P, and 8B3Q. The predicted structures of pIII, pVI, pVIII, pVII, pIX in the IM, and a prediction of the N1–N2 domains were drawn as described (Conners et al. 2023; Marvin et al. 2006; Rakonjac et al. 2024); pV, pink ovals; pI/pXI, purple shape. pIV structure (green) was derived from a published open-gate model of pIV (Conners et al. 2021).

These issues can be overcome by using Ff phage-derived nanorods, with a reduced genome size, that can make the Ff-derived particles (nanorods) up to 20-fold shorter than full-length phages. The small size of nanorods is advantageous for diffusion-dependent applications such as lateral flow assays, tissue targeting or internalisation into mammalian cells (Sattar et al. 2015; Tsedev et al. 2022). Nanorods also provide a safer alternative to standard Ff-derived vectors for medical and environmental applications. They are noninfectious, cannot replicate independently and lack antibiotic resistance genes or any other coding sequences (Cha et al. 2021; Conners et al. 2023; Sattar et al. 2015; Tsedev et al. 2022).

Construction of short nanorods is possible by separating initiation and termination functions of the *(+) ori*. This is accomplished, by having two *(+) ori* sequences, where a complete one (*[+] ori1*) is followed by the PS, and by a second truncated (+) origin (*[+] ori2*) that can only function as a terminator of (+) strand replication. Such a replication cassette has been used to produce short cssDNA (221 nt) corresponding to a small segment within a plasmid replicon, producing Ff-derived nanorods that are 50 nm in length (Specthrie et al. 1992).

To date, production systems for Ff-derived nanorods have been composed of either two plasmids, or a plasmid and a helper phage (Cha et al. 2021; Conners et al. 2023; Nafisi et al. 2018; Sattar et al. 2015). As a result, these nanorod production systems are labour-intensive, inefficient and time-consuming to use. To produce nanorods, two-plasmid transformation or transformation followed by helper phage infection is required. In the latter case, phages and nanorods are produced together; hence a complex purification protocol is required to separate the short nanorods from the longer helper phages. While two-plasmid systems eliminate a helper phage, they impose a requirement for nanorod production to be maintained over many generations after transformation of plasmids into the host. This poses a problem because filamentous phage replication drops dramatically after six generations (cell divisions) of the host bacterium (Lerner and Model 1981; Merriam 1977; Smeal et al. 2017), making it impractical to maintain production in transformed cell lines. Even if nanorod production is initiated at the time of transformation, the peak in production occurs about seven generations before the number of transformed cells increases sufficiently. For example, one transformation gives rise to ~10^7 transformed cells; if the production culture is 1 L in volume, 13 cell divisions are required to reach the optimal cell density of ~10^{11} cells per L, whereas replication from the f1 origin drops after six generations. Due to the early production peak and a finite number of f1-derived nanorods produced per cell, the per-volume yield of nanorods is expected to be much below the capacity of the system.

In this work we provide three key solutions to expedite and increase the efficiency of plasmid-based Ff-derived nanorod production: (i) conversion of a two-plasmid to a single-plasmid system, thereby simplifying the pre-production steps; (ii) inclusion of the Ff negative origin of replication in the nanorod replication-assembly cassette, increasing the copy number of the nanorod backbone cssDNA; (iii) conversion of nanorod cssDNA replication from constitutive to inducible to allow the transformed bacterial cell culture to grow before the nanorod production is induced, thus shifting the peak of nanorod production to a timepoint when the cell number is optimal. In summary, switching to a single-plasmid nanorod production system reduces the labour and antibiotic use during fermentation compared with the two-plasmid system, whereas the two latter improvements result in a 100-fold increase in nanorod production per-volume over the *(+)-ori*-only constitutive replication system.

2 | Experimental Procedures

2.1 | Bacterial Strains

Escherichia coli laboratory strains used in this work are K2091 and K2245. K2091 is a suppressor D (*supD*) strain, containing a L-seryl-tRNA^{serU} (*serU*) gene mutation *(SerU60)* where the anticodon CGA is mutated to CTA to become complementary to *amber* stop codon TAG. This mutation allows translation of the *amber* stop codon into serine [allele name is *serU60*(AS) or *supD60(AS)*]. In this work, *supD* strain K2091 is used for translation of *gVII-I^{am4}* mutant engineered to contain *amber* mutation instead of Ser codon at position 4. *serU60* in this *supD* mutant allows translation of the engineered *amber* codon into amino acid Ser, resulting in a wild-type protein sequence. K2091 genotype is *HfrC, S26 RIE, fadL701 phoM510 mcrB rrnB tonA22, garB10, ompF, relAl, pit10, spoT1, T2^R, lacI^q supD, zed508::Tn10* (Sattar et al. 2015). K2245, a strain lacking a suppressor mutation, does not produce pVIII due to the *gVIII^{am4}* mutation, thereby eliminating pVIII toxicity in the absence of nanorod assembly and was used for the construction and purification of pVIII-encoding plasmids. K2245 genotype is *Δ(araD-araB)567, ΔlacZ4787(::rrnB-3), λ-, ΔrecO737, rph-1, Δ(rhaD-rhaB)568, hsdR514; F′[::Tn10 proAB+ lacI^q Δ(lacZ)M15]* (Conners et al. 2023).

2.2 | Media and Growth Conditions

Bacteria were cultured in Difco 2×YT media (Becton-Dickinson, BD). Liquid cultures were incubated at 37°C with continuous shaking (200 rpm) unless otherwise stated. To make plates, media described above were solidified by adding agar (1.5% w/v). Antibiotics were supplemented when required at the following concentrations: kanamycin (Km) at 50 μg/mL; tetracycline (Tet) at 10 μg/mL.

2.3 | Recombinant DNA Technology Methods

General molecular biology and recombinant DNA techniques such as PCR, DNA restriction digests, ligation, DNA sequencing, DNA agarose gel electrophoresis, preparation of competent cells, transformation and purification of plasmid DNA were carried out as previously described (Sambrook and Russell 2001). DNA fragments for the construction of recombinant plasmids were either custom-synthesised or PCR-amplified. The pPop-up series of plasmids were constructed as described in Figures S2, S3, S5 and S7.

2.4 | Nanorod Production and Purification

For nanorod production, high-efficiency electrocompetent K2091 cells were transformed with a specific pPop-up single

nanorod-producing plasmid. After transformation cells were incubated for 1 h in 1 mL of SOC (Super Optimal broth with Catabolite repression). For antibiotic selection, transformed cells were suspended in 10 mL of liquid 2×YT media containing Km at 50 μg/mL. Resuspended cells (5 mL) were added to 500 mL of pre-warmed medium containing the same ingredients, in a 2 L flask and incubated overnight at 37°C with aeration. For the pPop-up or helper plasmids containing *gII* driven by the inducible *lacUV5* promoter, IPTG was added to the culture at $OD_{600} = 0.1$. After a 16-h incubation, the cells were removed from the culture by centrifugation (8000 *g* at 4°C). The culture supernatant was poured into sterile centrifuge bottles. Triton X-100 and Sarkosyl were added to 0.01% and incubated for 1 h at room temperature to solubilise the remaining membrane fragments in the culture supernatant. PEG8000 powder was added to 15% (w/v). After the PEG was dissolved, NaCl powder was added to 0.5 M, dissolved, and the suspension was incubated on ice for 2 h. The nanorods were then pelleted by centrifugation at 8000 *g* for 30 min at 4°C. The supernatant was decanted, and the centrifuge bottles were centrifuged again under the same conditions for 5 min to collapse the nanorod pellet to the bottom of the bottle. This is required because the nanorod PEG pellet precipitates during centrifugation as a sticky film along the wall of the bottle. The collapsed pellet was resuspended in 5 mL of 1×TBS (pH 7.6) and the remaining insoluble debris was pelleted by centrifugation at 8000 *g* for 30 min at 4°C. DNAse- and RNAse-containing buffer (final concentration 12 μg/mL DNase, 40 μg/mL RNase, 5 mM $MgCl_2$, 10 mM TRIS pH 8.0) was then added to the resuspended nanorod particles and incubated at room temperature for 1 h. DNAse and RNAse were inactivated by the addition of EDTA at a final concentration of 20 mM. Particles were repurified by precipitation in 15% (w/v) PEG, 0.5 M NaCl solution as described above. The nanorod pellet was resuspended in 0.5 mL 1×TBS (pH 7.6) and centrifuged again at 4000 *g* for 10 min at room temperature to remove the insoluble debris.

The nanorods were further purified by caesium chloride gradient centrifugation as described (Sattar et al. 2015). The nanorod-containing fractions devoid of cell-derived DNA or RNA were identified by agarose gel electrophoresis of SDS-disassembled nanorods. The fractions that contained the strongest nanorod cssDNA band, and no residual RNA and DNA, were combined and dialysed against 3000 volumes of 1× PBS or TBS or 50 mM Tris–HCl pH 8 buffer at 4°C, using 50 kDa cut-off Slide-a-Lyzer dialysis cassettes. Alternatively, the fractions were concentrated and desalted by spin-ultrafiltration through a 100 kDa cut-off membrane (Vivaspin) by centrifugation at 4500 *g* for 3 min. Samples were washed by adding new buffer four times, followed by a final centrifugation at which no buffer was added. Retentate containing purified nanorods was collected and stored at 4°C.

2.5 | Agarose Gel Electrophoresis of SDS-Disassembled Phage-Derived Nanorods and Quantification by Densitometry

Nanorods in purified samples were disassembled by mixing with SDS buffer (1% SDS, 1× TAE, 5% glycerol, 0.05% Brom-phenol blue) and heating at 99°C for 10 min. After equilibration to room temperature, the samples were loaded onto a 1.2% (w/v) agarose gel (1× TAE buffer, pH 8.3) and electrophoresis was run for 150 min at 3.7 V/cm. The gel was stained in Ethidium bromide for 20 min, followed by destaining, and imaging under UV light using a GelDoc system (Bio-Rad) (Rakonjac and Model 1998).

The released cssDNA was quantified by densitometry of EtBr-stained bands. To obtain a standard curve, each quantification gel was also loaded with a series of pure spectrophotometrically quantified cssDNA (Figures S4 and S6). This cssDNA standard was obtained by purification from nanorods using an M13 ssDNA purification protocol based on the silica spin columns (New England Biolabs).

On completion of electrophoresis the amount of cssDNA in all bands in gel images were analysed densitometrically using ImageJ software (NIH) as described (Rakonjac and Model 1998; Schneider et al. 2012). Microsoft Excel was used to plot the standard curve and quantify the cssDNA copy number of the samples which in turn corresponds to the number (titre) of the nanorods (Figures S4B and S6B).

2.6 | Staining and Transmission Electron Microscopy of Nanorods

All transmission electron microscopy images (micrographs) were collected at the Manawatū Microscopy and Imaging Centre (MMIC), College of Sciences, Massey University, Manawatū Campus. Purified nanorod samples were diluted in MilliQ water to a final concentration of 10^{10} nanorods/mL. An 80 μL sample drop was placed in a glass Petri dish lined with Parafilm (Bemis Company Inc., USA). A formvar/carbon-coated 200 mesh copper grid (Agar Scientific, coated in the lab) was placed film side down onto the sample droplet and left for 4 min to allow adsorption of nanorods onto the grid. The grid was carefully lifted and placed on the side of Whatman No1 filter paper to remove excess liquid.

The film with the adsorbed nanorods was placed on a drop of 2% uranyl acetate in MilliQ and incubated for 4 min at room temperature to stain. Excess fluid was wicked away, and the film was placed onto Whatman No1 paper to dry. Images were collected with a FEI Tecnai G2 Spirit BioTWIN Transmission Electron Microscope (TEM) equipped with a 2048×2048 pixels CCD camera (TVIPS TemCam-F224) at 100 kV. Magnifications were 30,000× (pixel size 0.45 nm at the specimen) or 67,000× (pixel size 0.21 nm at the specimen).

3 | Results

3.1 | Single-Plasmid Nanorod Production System

To simplify and accelerate the nanorod production procedure, we engineered a single-plasmid system (Figure 1). We combined all open reading frames coding for phage proteins and the replication-assembly cassette required for producing 50-nm nanorods (containing 221 nt circular ssDNA [cssDNA] backbone; Specthrie et al. 1992) into a single plasmid (Figure 2) we named pPop-upUni221. To construct this plasmid, the nanorod replication-assembly cassette (we named BSF, for Biological Scalable Ff-derived) was inserted into a helper plasmid upstream

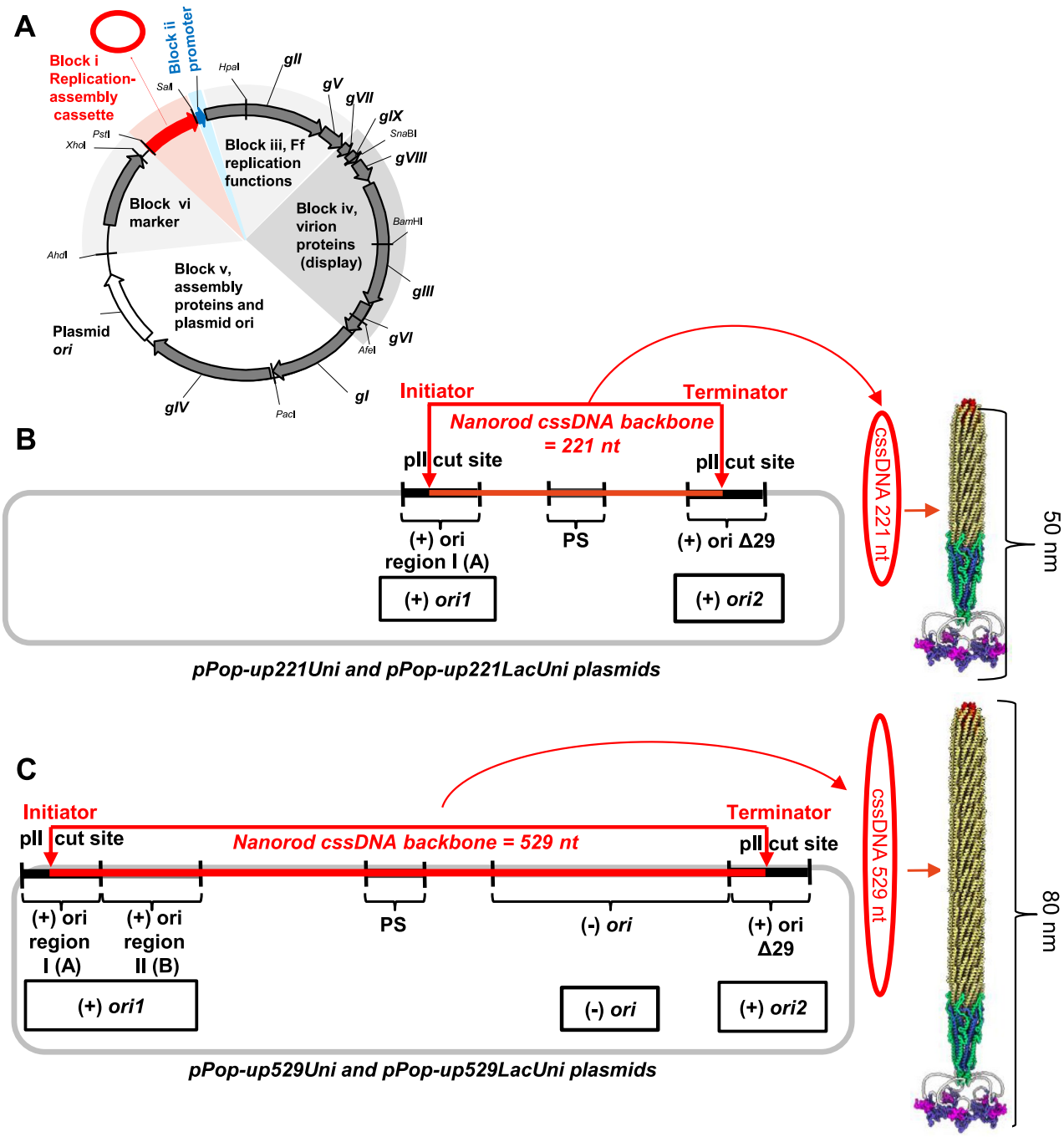

FIGURE 2 | Maps of the pPop-up plasmids and replication-assembly cassettes. (A) Functional blocks are indicated: (i) BSF replication-assembly cassette (red), template for replication of cssDNA that is the backbone of the nanorod; (ii) promoter (blue) driving the *gII*(*gX*)-*gV*-*gVII*-*gIX*-*gVIII* operon; (iii) replication genes *gII*-*gV*; (iv) virion genes (*gVIII*-*gVI*); (v) assembly-egress genes (*gI*-*gIV*) and plasmid origin of replication; (vi) selective marker. Construction of the Pop-up plasmids is described in Figures S2, S3, S5 and S7. (B, C) Schemes of the nanorod-producing pPop-up single plasmids including details of the replication-assembly cassettes. The resulting cssDNA (red ovals) and nanorods (structural models) are drawn on the right-hand side. (B) pPop-up221 plasmid series. The replication-assembly cassette BSFp contains (+) origins of replication (*ori1* and *ori2*) and packaging signal (PS). (C) pPop-up529 plasmid series. The replication-assembly cassette BSFpn contains (+) and (−) Ff origins of replication and packaging signal (PS).

of *gII*, coding for the replication protein pII (Figures 1, 2A, S2 and S3). The f1 virion proteins encoded by this plasmid were all wild-type, apart from *gVIII* that contained two mutations. The first mutation was TCT (Ser) codon 4 to *amber* stop codon, resulting in a phenotypically null mutant in nonsuppressor host strains. One purpose of this *amber* mutation is to avoid pVIII toxicity during cloning steps and production of plasmid DNA that we have performed in a suppressor-negative host strain (K2245). A second purpose is to reduce the amount of pVIII in the cells during nanorod production in suppressor D (*supD60 or serU60*) strain K2091 (Miller and Albertini 1983). Nanorods produced here had a more-than-10-fold shorter shaft and therefore required less than 10% of the pVIII for the assembly in comparison to Ff infection. The decreased amount of pVIII is due to the lower

efficiency of the *amber* codon translation in *supD* strains relative to that of the original sense codons (Miller and Albertini 1983). The amino acid sequence of suppressed *gVIII amber* mutant at codon 4, however, remains unchanged given that *supD* tRNA^{SerU60} incorporates a Ser residue at the *amber* codon. Another mutation was engineered in codon 44 (TAT; encoding Tyr 21 of the mature pVIII) to ATG (Met). This mutation has been shown previously to result in identical conformation of all copies of pVIII (in contrast to the wild-type where the subunits assume a slight difference in orientation relative to the virion helix axis) and has been used for structural analyses of Ff phages (Conners et al. 2023; Marvin et al. 2006).

A single transformation step of this new pPop-upUni221 plasmid (8857 nt in length) into an *E. coli supD* host (K2091) results in the production of all phage proteins, including pVIII, required for nanorod assembly. However, only a short fragment of the plasmid, corresponding to the nanorod replication-assembly cassette (221 nt), undergoes rolling circle replication between the Ff *(+) ori1* (initiator) and *(+) ori2* (terminator) to form short circular ssDNA. This template serves as the assembly axis for the production of 50 nm nanorods (Figures 2B and 4C).

The Pop-upUni221 plasmid is divided into six functional blocks which can be modified individually to change the properties of the production system or functionalities displayed on the nanorods (Figure 2A). This modular design allows for customisation for various applications, such as peptide or protein display, inclusion of chemical or enzymatic modification handles, or altering the length of the nanorods. Two blocks, corresponding to the replication-assembly cassette (Figure 2A, block i), and the promoter controlling expression of the gene encoding the Ff replication protein pII (Figure 2A, block ii), have been modified in this current work to increase nanorod production efficiency (see the sections below).

3.2 | Inclusion of the *(–) Ori* Into the Nanorod Replication-Assembly Cassette

The pPop-upUni221 single-plasmid production system contains a replication-assembly cassette variant we named BSFp, where 'p' stands for positive (*ori*); (Figure 2B; Specthrie et al. 1992). In this system, the cssDNA replication initiator corresponds to the first positive origin *[(+) ori1]* containing only the core (region A or I) of the positive-strand Ff origin of replication (Figure 2B). This *ori* provides a binding site for the Ff replication protein pII that cuts the (+) strand of double-stranded plasmid DNA at the pII recognition sequence GTTCTTT↓AATA, to form a primer for (+) strand cssDNA replication (Asano et al. 1999). It is followed by a packaging signal that is required for the cssDNA to serve as a backbone for the assembly of nanorods. The cassette ends with a terminator [*(+) ori2*], which is a truncated *(+) ori* mutant (*Δ29*) that does not support initiation of the (+) strand replication (Figure 2B). This arrangement only permits initiation of (+) strand replication at *(+) ori1*, followed by elongation past PS, and termination after 221 nt have been replicated, at *(+) ori2*. The termination of (+) strand replication is achieved by a pII-catalysed cut at GTTCTTT↓AATA within *(+) ori2*, coupled to ligation of the released (+) strand 3′-end with the 5′ end of the displaced (+) strand created at the initiation step, to produce a (+) strand cssDNA of 221 nt. The template dsDNA is reconstituted by joining between the 5′-P end (activated by covalent linkage to pII) generated at *ori2* and the 3′-end of the newly synthesised DNA (Asano et al. 1999; Horiuchi 1997; Moscoso et al. 1995; Ruiz-Maso et al. 2015; Valdelvira et al. 2021). The produced 221-nt (+) strand cssDNA serves as the structural and assembly backbone of the 50 nm nanorod (Specthrie et al. 1992). This design, however, only permits the 221-nt (+) strand cssDNA replication from the whole plasmid as a template, but prevents full rolling circle replication cycle of the nanorod's 'mini'-genome, thereby limiting the number of assembled nanorods (Figure 3A).

To overcome this limitation, we designed a pPop-up plasmid for increased nanorod production, by inclusion of *(–) ori* into its replication-assembly cassette which we named BSFpn ('pn' stands for positive and negative *ori*; Figure 2C). The inclusion of *(–) ori* within the cassette increased its length from 221 to 529 nt, hence the cost was a longer nanorod (80 nm vs. 50 nm; Figures 5 and 4). Another difference relative to the 221-nt BSFp cassette, was an extension of the initiator *[(+) ori1]* from containing region A (I) only to full length (Figure 2C), allowing increased binding of the replication protein pII (Dotto et al. 1984).

The *(–) ori* of the BSFpn cassette was expected to produce a substantially higher yield of nanorods than BSFp and other published cassettes lacking the *(–) ori* (Cha et al. 2021; Sattar et al. 2015; Specthrie et al. 1992) by allowing the replication of the nanorod backbone through the (–) strand. This would generate a higher number of short (+) strand cssDNA, leading to a higher yield of nanorods in comparison with the *(+)-ori*-only replication-assembly cassette (Figure 3A and 3B).

To test this hypothesis, production of nanorods from the two pPop-up plasmids, containing either the BSFp (BSFp221, 221-nt) or the BSFpn (BSFpn529, 529-nt) replication-assembly cassette, pPop-up221Uni and pPop-up529Uni (Figures S2 and S3), was compared under the same conditions of production and purification (Figure 3C). The yield of nanorods was quantified densitometrically from agarose gel electrophoresis of cssDNA encapsulated inside the purified nanorods (see Figure S4 for quantification gel, standard curve and details of quantification). pPop-up529Uni produced about 20-fold more nanorods than pPop-up221Uni, which contains a BSFp cassette ($4.9 \pm 0.3 \times 10^{14}$ and $2.4 \pm 0.2 \times 10^{13}$ per L, respectively; Table 1, Figure 3F). This finding demonstrates that the presence of the (–) *ori* in the replication-assembly cassette BSFpn increases nanorod production compared with the *(+)-ori*-only systems.

3.3 | Improvement of Nanorod Production by Engineering the Inducible-Replication System

To date, all helper phages and helper plasmids used in phage display technology have been based on constitutive replication, where the native (constitutive) Ff pA promoter drives expression of the replication protein pII. However, due to limitations in resources, chiefly DNA polymerase III required for replication of cssDNA, and the accumulation of pX, which inhibits pII-mediated initiation of replication from (+) *ori*, phage production drops after ~6–7 host cell divisions (Lerner and Model 1981; Merriam 1977; Smeal et al. 2017), despite constitutive expression of pII. This is a major limitation for plasmid-based nanorod production systems, making production from a transformant colony

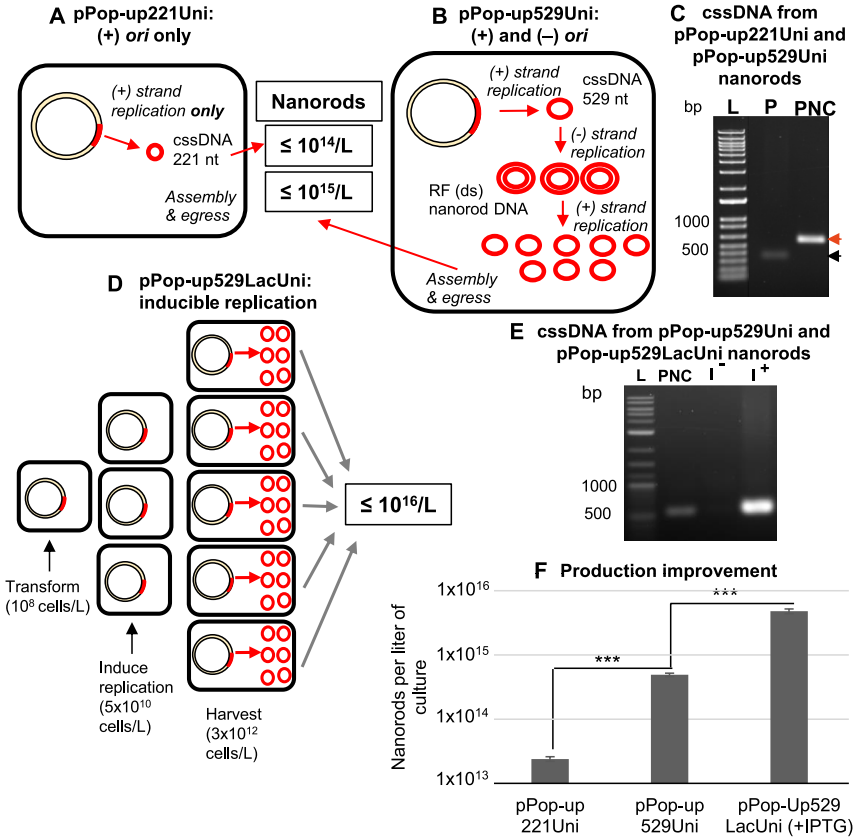

FIGURE 3 | Two improvements increasing nanorod production by two orders of magnitude. (A–C) Improved production of nanorods by inclusion of the (–) strand *ori* in the replication-assembly cassette. (A) Diagram of the nanorod cssDNA replication from a replication-assembly cassette containing only the *(+) ori* that results in only cssDNA production from the plasmid pPop-up221Uni as a template. (B) Diagram showing the effect of the *(–) ori* inclusion on nanorod production from pPop-up529Uni. Presence of *(–) ori* results in a cascade of multiple replication cycles of the BSFpn cassette replication and a ~10-fold increase in nanorod production. (C) Agarose gel electrophoresis of SDS-disassembled nanorods produced from the Pop-up plasmid containing only the *(+) ori* (P; pPop-up221Uni), or both *(+) ori* and *(–) ori* (PNC; pPop-up529Uni). L, 1 kb dsDNA marker; black arrow indicates nanorod cssDNA of 221 nt; red arrow 529 nt. (D, E) Further improvement of the nanorod production by the inducible production of replication protein pII. (D) A diagram showing how the induction of replication after the density of transformed cells increases results in the overall increased production of nanorods. (E) Agarose gel electrophoresis of SDS-disassembled nanorods produced from the Pop-up plasmids containing the BSFpn cassette (that includes both (+) and (–) replication origins). PNC; constitutive replication due to the constitutive Ff promoter pA driving expression of the gene encoding replication protein pII (pPop-up529Uni); Uninduced (I^-) and IPTG-induced (I^+) nanorod cssDNA replication from the pPop-up plasmid where the constitutive *pA* promoter was replaced by a *placUV5* inducible promoter (pPop-up529UniLac). Nanorods were produced from freshly electroporated culture of strain K2091, a *supD lacI*^{q} strain (see Section 2 for a complete genotype and protocols of nanorod production, purification and quantification). Lane I^+, nanorod production was induced by addition of IPTG (final concentration 100 μM) to the transformed cell culture at OD 0.1, followed by overnight incubation with aeration at 37°C. For nanorod production represented by lane I^-, no IPTG was added. (F) Comparison of pPop-up221Uni, pPop-up529Uni and pPop-up529UniLac nanorod production. Details of the nanorod quantification are shown in Figures S4 and S6 and Section 2. Standard deviations were derived from three technical replicates. *** indicates significance of $p < 0.0001$ (0.00002 for pPop-up221Uni vs. pPop-up529Uni and 0.00006 for pPop-up529Uni vs. pPop-up529UniLac) calculated using a two-tailed *t*-test.

(that takes at least 20 cell divisions to form) very poor. We hypothesised that delaying cssDNA replication in cultures of freshly transformed cells used for nanorod production could be beneficial. By postponing the peak of nanorod production until the cell population had amplified sufficiently, we could potentially avoid the poor nanorod yield as a result of per-cell production peaking before the transformed cells reach sufficiently high density (Figure 3D). This was achieved by introducing inducible expression of the gene encoding the replication protein pII (Figure S5). The constitutive 'native' phage promoter *pA* was replaced with the *placUV5* promoter, generating the pPop-upLac series of the single-plasmid nanorod production vectors (Figures S5 and S7). The *placUV5* promoter is insensitive to catabolic repression by glucose (Silverstone et al. 1970), hence the nanorod production is inducible even in the presence of glucose in the medium. The inducible-replication plasmid (named pPop-up529LacUni) carried the same BSFpn cassette [529 nt, containing *(–) ori*, and producing 80-nm nanorods] as the original constitutive-pII-expression pPop-up plasmid (pPop-up529Uni). Production of nanorods from these two plasmids, pPop-up529Uni (constitutive) and pPop-up529LacUni (inducible) was compared to examine whether the delayed phage replication results in an overall increase in the total number of nanorods produced (Figure 3E). A ~10-fold increase in nanorod production was seen in the culture of pPop-up529LacUni to which IPTG was added in comparison to the nanorods produced using the constitutively replicating

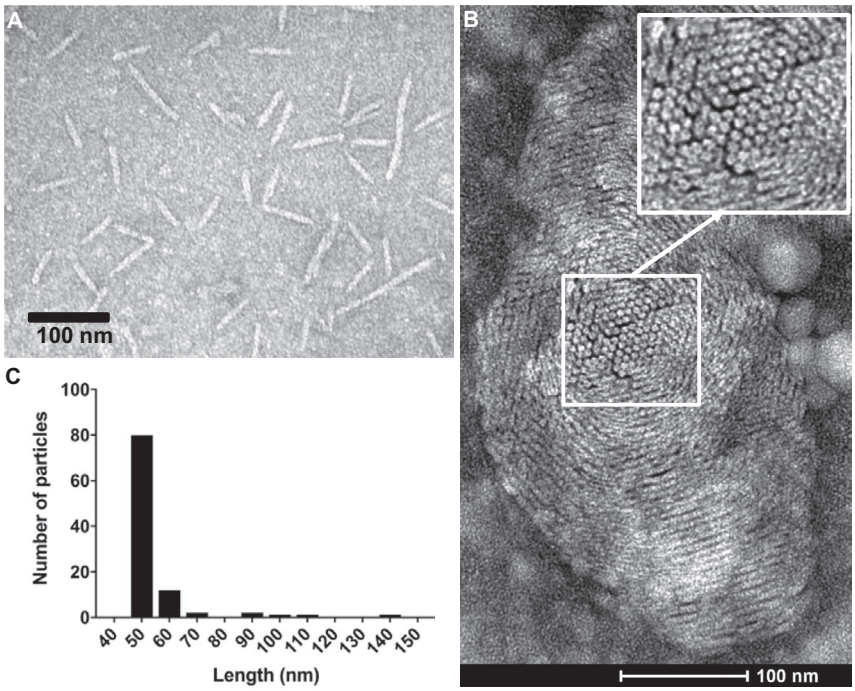

FIGURE 4 | Transmission electron micrographs and size distribution of 221-nt nanorods. (A, B) Transmission electron micrographs of purified negatively stained 221-nt (50 nm) nanorods. In B, the nanorods form a crystalline array on the grid with the nanorods in the centre being orthogonal to the grid surface (inset). (C) Histogram of nanorod length distribution plotted from the length measurements of 100 well-separated particles using ImageJ software. Samples were prepared for TEM by staining on the grid with uranyl acetate and imaged as described in Section 2.

TABLE 1 | Nanorod production from a single-plasmid system.

Plasmid[a]	*(–) ori*[b]	Nanorod backbone cssDNA (nt)[c]	Nanorod length (nm)	Expression of *gII*(*gX*)-*gV*-(*gVII*-*gIX*-*gVIII*) *operon*	Nanorods per litre of culture[d]
pPop-up221Uni	No	221	50	*pA* (constitutive)	$2.4 \pm 0.2 \times 10^{13}$
pPop-up529Uni	Yes	529	80	*pA* (constitutive)	$4.9 \pm 0.3 \times 10^{14}$
pPop-Up529LacUni (–IPTG)	Yes	529	80	*placUV5*, not induced	$9.7 \pm 0.4 \times 10^{13}$
pPop-up529LacUni (+IPTG)	Yes	529	80	*placUV5*, induced	$4.8 \pm 0.4 \times 10^{15}$
pPop-up221LacUni (+IPTG)	No	221	50	*placUV5*, induced	$1.9 \pm 0.1 \times 10^{14}$

[a]pPop-up plasmids. Number indicates the size of the nanorod cssDNA backbone (in nucleotides); Lac indicates *placUV5* promoter upstream of *gII*; Uni indicates wild-type (f1) virion proteins apart from pVIII Tyr to Met mutation at position 21 of the mature portion of pVIII. All plasmids encode all Ff (f1-derived) proteins. Apart from a Tyr 21 Met mutation in pVIII, two additional coding sequence mutations are *gII* IR1-B(C143T) and $gVIII^{4am}$. $gVIII^{4am}$ indicates *amber* stop codon (Ser −20) in the signal sequence. In the SupD suppressor host used for nanorod production, the *amber* codon is read as Ser. pPop-up plasmids also contain a plasmid origin of replication (pA15) and a selective marker (Km^R); see the map in Figures S2, S3, S5 and S7.
[b]Presence of the negative Ff origin [*(–) ori*] in the replication-assembly cassette.
[c]Size (in nucleotides) of the circular ssDNA (nanorod backbone) produced from the replication-assembly cassette.
[d]Yield of pure nanorods after CsCl gradient centrifugation as described in Section 2.

pPop-up529Uni plasmid ($4.8 \pm 0.4 \times 10^{15}$ vs. $4.9 \pm 0.3 \times 10^{14}$ nanorods per 1 L of culture, respectively; Table 1, Figure 3F; see Figure S6 for quantification gel, standard curve and details of quantification). A smaller number of nanorods was produced by the pPop-up529LacUni in the absence of IPTG, indicating there was background expression of pII from the uninduced *placUV5* promoter ($9.7 \pm 0.4 \times 10^{13}$ nanorods per 1 L of culture; Table 1). Introduction of inducible replication into the *(+) ori*-only pPop-up plasmid, to construct pPop-up221LacUni (Figure S7), which produced 50 nm nanorods (Figure 4), also increased the yield by an order of magnitude relative to the constitutive pPop-up221Uni (Table 1).

TEM analyses showed that in both the 50 and 80 nm nanorod preparations (Figures 4A and 5A), >90% of the particles were within ±10 nm of their expected length (Figures 4C and 5C). Interestingly, high-concentration purified nanorods spontaneously formed higher-order structures after storage at 4°C for

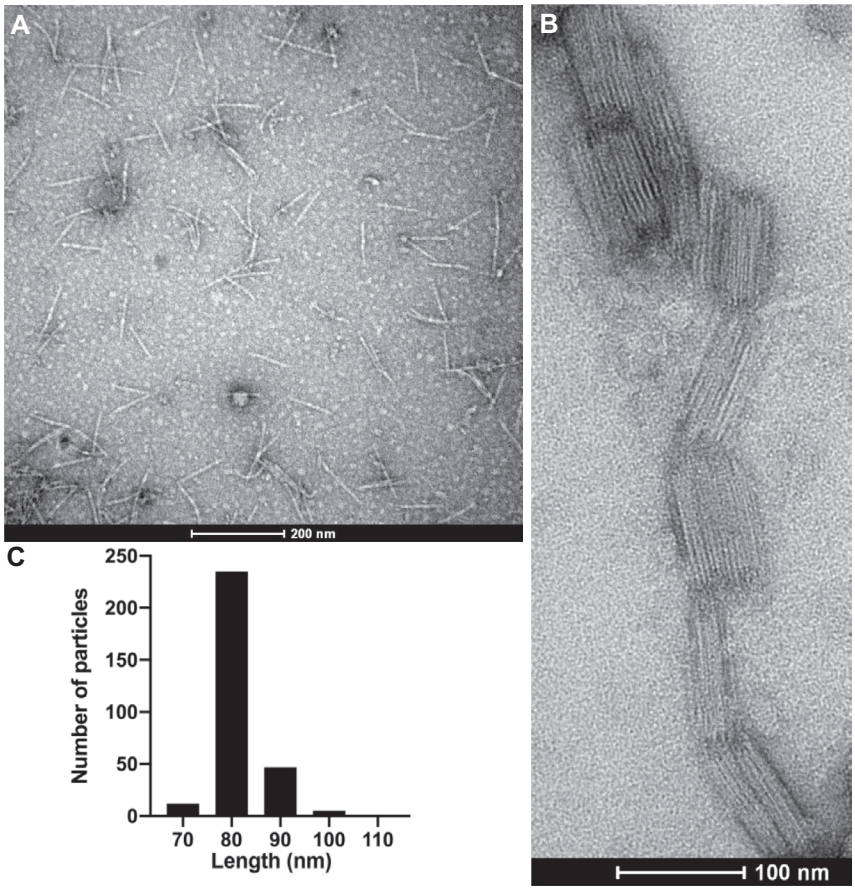

FIGURE 5 | Transmission electron micrographs and size distribution of 529-nt nanorods. (A, B) Transmission electron micrographs of purified negatively stained 529-nt (80 nm) nanorods. (C) Histogram of the nanorod length distribution plotted from the length measurements of 300 well-separated particles using ImageJ software. Samples were prepared for TEM by staining on the grid with uranyl acetate and imaged as described in Section 2.

6 months or longer in a phosphate buffer containing 150 mM NaCl (diluted to 1.5 mM before application to the grid and staining), as observed by TEM of stained nanorods (Figures 4B and 5B). The 80 nm nanorods produced ribbon-like arrayed stacks (Figure 5B), whereas the 50 nm nanorods produced 2D crystalline rafts of nanorods (Figure 4B), with individual particles in the centre of the raft being orthogonal to the grid, forming a regular crystalline-like array (Figure 4B, see inset). This is a novel property in contrast to full-length Ff phages which require high concentrations of polymers such as dextran and PEG in order to form rafts and other higher-level 3D or 2D structures (Balchunas et al. 2019; Dogic and Fraden 2001). Such Ff structures are an important model of colloidal membranes in the field of soft matter physics (Dogic 2016; Sharma et al. 2014).

4 | Discussion

In this report, we describe a novel single-plasmid system for production of filamentous phage Ff-derived nanorods. Our single-plasmid system allows for simple and efficient single-step production of Ff-derived nanorods of uniform length. This is in contrast to the currently used two-plasmid-based nanorod production systems that require two sequential transformations, or a single transformation resulting in low-frequency double-transformed cells (Cha et al. 2021; Conners et al. 2023; Nafisi et al. 2018; Sattar et al. 2015). The single-plasmid system, therefore, simplifies plasmid-based nanorod production for applications such as vaccines, diagnostics or therapeutics.

We next expanded the replication-assembly cassette by inserting the *(−) ori*, which allowed replication of the short cssDNA excised from the pPop-up529Uni plasmid, resulting in an increase in nanorod production by an order of magnitude. Increased production in these constructs may also be partly due to extending *(+) ori1* from containing only the essential A(I) region in BSFp to the full *(+) ori1* in BSFpn. This extension is known to improve the binding of pII to the initiator (Dotto and Zinder 1984; Enea and Zinder 1982). The pPop-up plasmids, however, contain a *gII IR1-B*(*C143T*) mutation encoding a pII (Thr182Ile) variant, reported to compensate for truncated *(+) ori* containing only the 'core' region A in the helper phage-based nanorod production system; hence the effect of extension of the *(+) ori* sequence to include region A in the pPop-up529 plasmid is expected to be much smaller than for the wild-type pII-mediated replication (Sattar et al. 2015).

Use of a replication-assembly cassette containing the *(−) ori* has been reported previously (Nafisi et al. 2018). However, in this case one of the two origins of the replication-assembly cassette corresponded to a complete Ff intergenic sequence [packaging signal, (−) *ori* and (+) *ori*]. The cassette was significantly larger than that of BSFpn and could easily recombine with the terminator due to duplication of both *ori's*, explaining the reported production of longer-size particles (Nafisi et al. 2018). It has also

been reported that the truncated *Δ29* (+) *ori* [used here as the *(+) ori2* or the terminator] is a poor terminator and can also initiate replication. This was reported as a cause of up to 50% of cssDNA being produced from replication initiating at (+) *ori2Δ29* (Cha et al. 2021; Nafisi et al. 2018). However, long cssDNA molecules that terminate beyond the (+) *ori2Δ29* were not observed in our two-plasmid system (Conners et al. 2023) or in the pPop-up plasmids reported here (Figure 3C,E), where the replication cassette includes (−) *ori* (BSFpn). Even in the pPop-upUni221 plasmid with positive origin-only BSFp cassette, longer-than-expected cssDNA was not detected (Figure 3C).

Another key difference between our new system and those reported previously is that we used a suppressed *gVIII amber* mutant. By using a nonsuppressor host during the construction and purification of the pPop-up plasmid, we completely eliminated pVIII toxicity (Pratt et al. 1969; Schwartz and Zinder 1968). This approach also minimised the toxicity of pVIII during nanorod production in the *supD* host. SupD (SerU) only partially suppresses the *amber* stop codon, thus less unassembled pVIII accumulates in the cell than if wild-type pVIII were produced at wild-type levels. Given that the short nanorods produced here, 50 and 80 nm in length are ~5% and 10% of the full-length phage length, < 10% of the pVIII is needed to coat the short nanorods relative to the full-length phage production. In contrast, in the nanorod production setups where the full amount of pVIII inherent to the normal phage infection (wild-type *gVIII*) is produced, there is an excess of pVIII; hence the selective pressure against its toxicity is expected to favour growth of the cells containing mutant segregants that produce longer cssDNA backbone. Such mutants can arise during plasmid construction and on the passaging of transformed producer cells (Sattar et al. 2015). When compared to our stable nanorod production system, the reported inefficient termination at [*(+) oriΔ29*] and production of a large proportion of 'runaway' long nanorods (Cha et al. 2021; Nafisi et al. 2018; Praetorius et al. 2017; Shepherd et al. 2019) is likely to be attributable to combination of selective pressures. These include selection for longer templates that deplete most of the cellular pVIII and thereby relieve toxicity, and/or recombination that completely eliminates the terminator [*(+) oriΔ29*].

Production of nanorods was increased by another order of magnitude by the introduction of inducible replication from the *(+) ori*, by placing the gene encoding replication protein pII under the control of an inducible promoter (Figure 3D,E, Table 1). The two modifications together, inclusion of *(−) ori* into the replication-assembly cassette and inducible replication, increased the production overall by two orders of magnitude.

High-efficiency production resulted in high-density nanorod samples and spontaneous formation of higher-order structures from the nanorods, such as rafts on the TEM grid by the 50 nm nanorods and stacks of rods by the 80 nm nanorods. These properties are likely to be of interest for material science applications and the use of nanorods as a model in soft matter physics (Dogic 2016; Sharma et al. 2014).

Overall, the single-plasmid inducible system described here increased the per-volume production by as much as two orders of magnitude relative to the widely used *(+) ori*-only systems. Moreover, it simplified production; by requiring only one transformation with a single plasmid. It also reduced the antibiotic use for production by having only one rather than two antibiotic resistance markers compared to all current two-replicon nanorod production systems. These advantages make the inducible single-plasmid system more suitable for the production of large volumes of pure nanorods that are typically required for biotechnological and biomedical applications of these biological nanoparticles.

Author Contributions

Rayén Ignacia León-Quezada: writing – original draft, investigation, formal analysis, visualization. **Majela González Miró:** methodology, writing – review and editing, investigation. **Sofia Khanum:** methodology, investigation, writing – review and editing. **Andrew J. Sutherland-Smith:** writing – review and editing, resources, supervision. **Vicki A. M. Gold:** visualization. **Jasna Rakonjac:** conceptualization, visualization, writing – review and editing, writing – original draft, methodology, investigation, supervision, project administration, funding acquisition, resources, formal analysis, data curation.

Acknowledgements

We are indebted to Marjorie Russel for advice and comments throughout this project, and for the review of the manuscript. Manawatū Microscopy and Imaging Centre (Massey University, College of Sciences) is acknowledged for the Transmission Electron Microscopy service. RIL-Q, MGM and SK were supported by a generous donation from Anne & Bryce Carmine. Funding to VAMG from a Wellcome (Seed Award in Science; 210363/Z/18/Z) and to JR from Anonymous Donor, Palmerston North Medical Research Foundation, Massey University Research Fund and School of Natural Sciences; Royal Society Te Apārangi; Marsden Fund (03-MAU-210) is gratefully acknowledged. Open access publishing facilitated by Massey University, as part of the Wiley - Massey University agreement via the Council of Australian University Librarians.

Conflicts of Interest

The authors declare no conflicts of interest.

Data Availability Statement

The data that support the findings of this study are available from the corresponding author upon reasonable request.

References

Asano, S., A. Higashitani, and K. Horiuchi. 1999. "Filamentous Phage Replication Initiator Protein gpII Forms a Covalent Complex With the 5′ End of the Nick It Introduced." *Nucleic Acids Research* 27: 1882–1889.

Balchunas, A. J., R. A. Cabanas, M. J. Zakhary, et al. 2019. "Equation of State of Colloidal Membranes." *Soft Matter* 15: 6791–6802.

Cha, T. G., U. Tsedev, A. Ransil, et al. 2021. "Genetic Control of Aerogel and Nanofoam Properties, Applied to Ni-MnOx Cathode Design." *Advanced Functional Materials* 31: 2010867.

Conners, R., R. I. Leon-Quezada, M. McLaren, et al. 2023. "Cryo-Electron Microscopy of the f1 Filamentous Phage Reveals Insights Into Viral Infection and Assembly." *Nature Communications* 14: 2724.

Conners, R., M. McLaren, U. Lapinska, et al. 2021. "CryoEM Structure of the Outer Membrane Secretin Channel pIV From the f1 Filamentous Bacteriophage." *Nature Communications* 12: 6316.

Dogic, Z. 2016. "Filamentous Phages as a Model System in Soft Matter Physics." *Frontiers in Microbiology* 7: 1013.

Dogic, Z., and S. Fraden. 2001. "Development of Model Colloidal Liquid Crystals and the Kinetics of the Isotropic-Smectic Transition." *Philosophical Transactions of the Royal Society A* 359: 997–1014.

Dotto, G. P., K. Horiuchi, and N. Zinder. 1984. "The Origin of DNA Replication of Bacteriophage f1 and Its Interaction With the Phage Gene II Protein." In *Proteins Involved in DNA Replication*, edited by U. Huebscher and S. Spadari, 185–191. Plenum Publishing Corporation.

Dotto, G. P., and N. D. Zinder. 1984. "Reduction of the Minimal Sequence for Initiation of DNA Synthesis by Qualitative or Quantitative Changes of an Initiator Protein." *Nature* 311: 279–280.

Enea, V., and N. D. Zinder. 1982. "Interference Resistant Mutants of Phage f1." *Virology* 122: 222–226.

Haase, M., L. Tessmer, L. Köhnlechner, and A. Kuhn. 2022. "The M13 Phage Assembly Machine Has a Membrane-Spanning Oligomeric Ring Structure." *Viruses* 14: 1163.

Horiuchi, K. 1997. "Initiation Mechanisms in Replication of Filamentous Phage DNA." *Genes to Cells* 2: 425–432.

Lerner, T. J., and P. Model. 1981. "The "Steady State" of Coliphage f1: DNA Synthesis Late in Infection." *Virology* 115: 282–294.

Mai-Prochnow, A., J. G. Hui, S. Kjelleberg, J. Rakonjac, D. McDougald, and S. A. Rice. 2015. "Big Things in Small Packages: The Genetics of Filamentous Phage and Effects on Fitness of Their Host." *FEMS Microbiology Reviews* 39: 465–487.

Mao, C., D. Solis, B. Reiss, et al. 2004. "Virus-Based Toolkit for the Directed Synthesis of Magnetic and Semiconducting Nanowires." *Science* 303: 213–217.

Marvin, D. A., L. C. Welsh, M. F. Symmons, W. R. Scott, and S. K. Straus. 2006. "Molecular Structure of Fd (f1, M13) Filamentous Bacteriophage Refined With Respect to X-Ray Fibre Diffraction and Solid-State NMR Data Supports Specific Models of Phage Assembly at the Bacterial Membrane." *Journal of Molecular Biology* 355: 294–309.

McCafferty, J., A. D. Griffiths, G. Winter, and D. J. Chiswell. 1990. "Phage Antibodies: Filamentous Phage Displaying Antibody Variable Domains." *Nature* 348: 552–554.

Merriam, V. 1977. "Stability of the Carrier State in Bacteriophage M13-Infected Cells." *Journal of Virology* 21: 880–888.

Miller, J. H., and A. M. Albertini. 1983. "Effects of Surrounding Sequence on the Suppression of Nonsense Codons." *Journal of Molecular Biology* 164: 59–71.

Model, P., and M. Russel. 1988. "Filamentous Bacteriophage." In *The Bacteriophages*, edited by R. Calendar, 375–456. Plenum Publishing.

Moscoso, M., G. del Solar, and M. Espinosa. 1995. "Specific Nicking-Closing Activity of the Initiator of Replication Protein RepB of Plasmid pMV158 on Supercoiled or Single-Stranded DNA." *Journal of Biological Chemistry* 270: 3772–3779.

Nafisi, P. M., T. Aksel, and S. M. Douglas. 2018. "Construction of a Novel Phagemid to Produce Custom DNA Origami Scaffolds." *Synthetic Biology* 3, no. 1: ysy015. https://doi.org/10.1093/synbio/ysy015.

Praetorius, F., B. Kick, K. L. Behler, M. N. Honemann, D. Weuster-Botz, and H. Dietz. 2017. "Biotechnological Mass Production of DNA Origami." *Nature* 552: 84–87.

Pratt, D., H. Tzagoloff, and J. Beaudoin. 1969. "Conditional Lethal Mutants of the Small Filamentous Coliphage M13. II. Two Genes for Coat Proteins." *Virology* 39: 42–53.

Rakonjac, J. 2022. "Filamentous Bacteriophages: Biology and Applications." *eLS* 1–15. https://doi.org/10.1002/9780470015902.a9780470029482.

Rakonjac, J., J. Feng, and P. Model. 1999. "Filamentous Phage Are Released From the Bacterial Membrane by a Two-Step Mechanism Involving a Short C-Terminal Fragment of pIII." *Journal of Molecular Biology* 289: 1253–1265.

Rakonjac, J., V. A. M. Gold, R. I. Leon-Quezada, and C. H. Davenport. 2024. "Structure, Biology, and Applications of Filamentous Bacteriophages." *Cold Spring Harbor Protocols* 202: pdb.over107754.

Rakonjac, J., and P. Model. 1998. "Roles of pIII in Filamentous Phage Assembly." *Journal of Molecular Biology* 282: 25–41.

Roux, S., M. Krupovic, R. A. Daly, et al. 2019. "Cryptic Inoviruses Revealed as Pervasive in Bacteria and Archaea Across Earth's Biomes." *Nature Microbiology* 4: 1895–1906.

Ruiz-Maso, J. A., N. C. Macho, L. Bordanaba-Ruiseco, M. Espinosa, M. Coll, and G. Del Solar. 2015. "Plasmid Rolling-Circle Replication." *Microbiology Spectrum* 3: PLAS-0035-2014.

Russel, M., and P. Model. 1989. "Genetic Analysis of the Filamentous Bacteriophage Packaging Signal and of the Proteins That Interact With It." *Journal of Virology* 63: 3284–3295.

Sambrook, J., and D. W. Russell. 2001. *Molecular Cloning: A Laboratory Manual*. 3rd ed. Cold Spring Harbor.

Sattar, S., N. J. Bennett, W. X. Wen, et al. 2015. "Ff-Nano, Short Functionalized Nanorods Derived From Ff (f1, Fd, or M13) Filamentous Bacteriophage." *Frontiers in Microbiology* 6: 316.

Schneider, C. A., W. S. Rasband, and K. W. Eliceiri. 2012. "NIH Image to ImageJ: 25 Years of Image Analysis." *Nature Methods* 9: 671–675.

Schwartz, F. M., and N. D. Zinder. 1968. "Morphological Changes in *Escherichia coli* Infected With the DNA Bacteriophage fl." *Virology* 34: 352–355.

Scott, J. K., and G. P. Smith. 1990. "Searching for Peptide Ligands With an Epitope Library." *Science* 249: 386–390.

Sharma, P., A. Ward, T. Gibaud, M. F. Hagan, and Z. Dogic. 2014. "Hierarchical Organization of Chiral Rafts in Colloidal Membranes." *Nature* 513: 77–80.

Shepherd, T. R., R. R. Du, H. Huang, E. C. Wamhoff, and M. Bathe. 2019. "Bioproduction of Pure, Kilobase-Scale Single-Stranded DNA." *Scientific Reports* 9: 6121.

Silverstone, A. E., R. R. Arditti, and B. Magasanik. 1970. "Catabolite-Insensitive Revertants of *Lac* Promoter Mutants." *Proceedings of the National Academy of Sciences of the United States of America* 66: 773–779.

Smeal, S. W., M. A. Schmitt, R. R. Pereira, A. Prasad, and J. D. Fisk. 2017. "Simulation of the M13 Life Cycle II: Investigation of the Control Mechanisms of M13 Infection and Establishment of the Carrier State." *Virology* 500: 275–284.

Smith, G. P. 1985. "Filamentous Fusion Phage: Novel Expression Vectors That Display Cloned Antigens on the Virion Surface." *Science* 228: 1315–1317.

Specthrie, L., E. Bullitt, K. Horiuchi, P. Model, M. Russel, and L. Makowski. 1992. "Construction of a Microphage Variant of Filamentous Bacteriophage." *Journal of Molecular Biology* 228: 720–724.

Tsedev, U., C. W. Lin, G. T. Hess, J. N. Sarkaria, F. C. Lam, and A. M. Belcher. 2022. "Phage Particles of Controlled Length and Genome for *In Vivo* Targeted Glioblastoma Imaging and Therapeutic Delivery." *ACS Nano* 16: 11676–11691.

Valdelvira, R., L. Bordanaba-Ruiseco, C. Martin-Huestamendia, J. A. Ruiz-Maso, and G. Del Solar. 2021. "Acidic pH Decreases the Endonuclease Activity of Initiator RepB and Increases the Stability of the Covalent RepB-DNA Intermediate While Has Only a Limited Effect on the Replication of Plasmid pMV158 in *Lactococcus lactis*." *Frontiers in Molecular Biosciences* 8: 634461.

Vieira, J., and J. Messing. 1987. "Production of Single-Stranded Plasmid DNA." *Methods in Enzymology* 153: 3–11.

Supporting Information

Additional supporting information can be found online in the Supporting Information section.